

# Magnetic catalysis (and inverse catalysis) at finite temperature in two-color lattice QCD

E.-M. Ilgenfritz

*Joint Institute for Nuclear Research, VBLHEP, 141980 Dubna, Russia*

M. Müller-Preussker, B. Petersson, and A. Schreiber

*Humboldt-Universität zu Berlin, Institut für Physik, 12489 Berlin, Germany*

(Dated: October 29, 2013)

Two-color lattice QCD with  $N_f = 4$  staggered fermion degrees of freedom (no rooting trick is applied) with equal electric charge  $q$  is studied in a homogeneous magnetic background field  $B$  and at non-zero temperature  $T$ . In order to circumvent renormalization as a function of the bare coupling we apply a fixed-scale approach. We study the influence of the magnetic field on the critical temperature. At rather small pseudo-scalar meson mass ( $m_\pi \approx 175$  MeV  $\approx T_c(B=0)$ ) we confirm *magnetic catalysis* for sufficiently strong magnetic field strength, while at  $T = 195$  MeV and weak magnetic field ( $qB \lesssim 0.8$  GeV<sup>2</sup>) we find a rise of the Polyakov loop with  $qB$  and thus, indications for an *inverse magnetic catalysis*.

## I. INTRODUCTION

The interaction of strong magnetic fields with hadronic matter has recently been widely discussed because of its relevance to non central heavy ion collisions. In such collisions there will be two lumps of spectators moving in opposite directions. They give rise to a magnetic field perpendicular to the reaction plane, which may be estimated from the Lienard-Wiechert potentials of the moving spectators. From these estimates it can be shown that the magnetic field is so strong that its consequences cannot be studied perturbatively. In fact, the field is estimated to have strength  $eB \sim m_\pi^2 \sim 10^{18}$  Gauss at RHIC and LHC at the time of formation of the fireball. The field strength falls for large time  $t$  at most as  $1/t^2$  and because of conductivity effect may reach a plateau [1–3]. Therefore, for a longer time reaching from the formation of the fireball to the final transition from quark-gluon to hadron matter, it may be a reasonable approximation to assume a constant external field exerting influence on the transition.

It is known since a long time that the problem of a relativistic particle in a constant external magnetic field with spin 0 or 1/2 can be solved exactly [4–6]. With the help of these solutions one can discuss the effect in the Nambu-Jona-Lasinio [7] or in the chiral [8] model at zero temperature. The general result is that the magnetic field induces an increase of the chiral condensate. This was dubbed *magnetic catalysis* in Ref. [9] and claimed to be essentially model independent. For a recent review see [10]. The model calculations have been extended to finite temperature, in order to study the phase diagram of strongly interacting matter in a constant magnetic field. In this case there is no claim of model independence. The critical temperature of the chiral phase transition rises in most calculations [11]. There are also claims that the chiral and the deconfinement phase transitions split, and the

latter decreases with the magnetic field strength [12].

Recently several groups have started to investigate the problem through ab initio lattice simulations of QCD and QCD-like theories in a constant external magnetic field. There is no sign problem in contrast to e.g. the introduction of a chemical potential in QCD. The pioneering work was performed by M. Polikarpov and collaborators [13–16]. They carried out their calculations in quenched  $SU(2)$ . In our previous paper [17] we extended the calculations to  $SU(2)$  with four flavors of dynamical fermions. The choice of four flavors eliminates the need for rooting of the Kogut-Susskind or staggered fermion action. We observed *magnetic catalysis* for all temperatures investigated. The deconfinement transition, which we determined from the behavior of the Polyakov loop and the various parts of the gluonic action coincided within our precision with the chiral transition. The transition temperature increased with increasing magnetic field. However, in our calculations the temperature dependence was studied only by varying the bare coupling parameter  $\beta$ , while the magnetic field strength as well as the fermion mass was fixed in lattice units. As a consequence the physical field strength as well as the fermion mass was increasing with the temperature. This problem is removed in our present paper.

In the meantime, two groups have performed simulations in full QCD ([18–20] and [21–25]). Both groups observe *magnetic catalysis* for temperatures in the confined phase. Near the phase transition the second group observes what they call *inverse magnetic catalysis*, i.e. the chiral condensate and thus the transition temperature decreases with increasing magnetic field strength [21]. It is still not completely clear, whether the discrepancy is explained by the different sets of quark masses used. In [19] the case of two flavors is treated and the parameters chosen lead to a pion mass of approximately 200 MeV. In [21] the parameters and the action used are the same as in [26], namely  $2 + 1$

flavors with the parameters chosen to give the physical mass to the Goldstone pion connected to the exact lattice axial symmetry  $U(1)$ . In both calculations, the fourth root of the fermion determinants is taken to reduce the number of flavors (also called tastes). This procedure is still under debate. A nice recent review of the lattice results for QCD and QCD-like theories in external fields can be found in Ref. [27].

In this article we extend our calculations in [17] of the four-flavor, two-color theory to a considerably smaller value of the bare quark mass. In fact, now the ratio of the Goldstone pion mass to the critical temperature is similar to the physical case of QCD. Furthermore, we use the fixed-scale approach, which means that the lattice spacing dependence of the renormalization factors is irrelevant for our results. We measure the various parts of the gluon action, the Polyakov loop and the chiral condensate. With the help of these measurements we localize the finite temperature transition, and describe its dependence on the magnetic field strength. Although our model is not QCD, the chiral properties are quite similar. Furthermore, investigations of the dynamical  $SU(2)$  theory are of considerable interest, because they can eventually be extended to finite chemical potential without a sign problem. It is also easier to investigate the topological structure of the lattice gauge fields than in the  $SU(3)$  case.

In section II, for completeness, we specify the action and the order parameters, although they are the same as in our previous calculation [17]. In Section III we describe the simulation parameters, and in Section IV the scale determination. Section V is devoted to a presentation of our finite temperature results. Finally, in Section VI we discuss the results, compare with results of other groups, and present our conclusions.

## II. SPECIFICATION OF THE ACTION AND ORDER PARAMETERS

The theory, which we have chosen to investigate, is color  $SU(2)$  with four fermion flavors. We want to study its behavior at finite temperature under the influence of a strong external magnetic field. To this end we perform numerical simulations in the lattice regularization, which are fully non-perturbative also in the electromagnetic coupling to the magnetic field. The details of the corresponding model on the lattice are given in [17]. For completeness we present again the main building blocks here.

We introduce a lattice of four dimensional size

$$\mathcal{V} \equiv N_\tau \times N_\sigma^3. \quad (1)$$

The sites are enumerated by  $n = (n_1, n_2, n_3, n_4)$ , where the  $n_i$  are integers,  $n_i = 1, 2, \dots, N_\sigma$  for  $i =$

$1, 2, 3$  and  $n_4 = 1, 2, \dots, N_\tau$ . The fourth direction is taken as the Euclidean time direction. The lattice spacing is denoted by  $a$ . The physical volume  $V$  and the temperature  $T$  of the system are given by

$$V = (aN_\sigma)^3, \quad (2)$$

$$T = \frac{1}{aN_\tau}. \quad (3)$$

On the links  $n \rightarrow n + \hat{\mu}$  we define group elements  $U_\mu(n) \in SU(2)$ , where  $\mu = 1, 2, 3, 4$ . The boundary conditions of the  $U$ -fields are periodic. For the gauge part of the action we choose the usual Wilson action,

$$S_G = \beta \mathcal{V} \sum_{\mu < \nu} P_{\mu\nu}, \quad (4)$$

where

$$P_{\mu\nu} = \frac{1}{\mathcal{V}} \sum_n \left( \frac{1}{2} \text{Tr} (1 - U_{\mu\nu}(n)) \right) \quad (5)$$

with  $U_{\mu\nu}(n)$  denoting the  $\mu\nu$ -plaquette matrix attached to the site  $n$ .

For the fermion part of the action, we use staggered fermions, which are spinless Grassmann variables  $\bar{\psi}(n)$  and  $\psi(n)$  being vectors in the fundamental representation of the gauge group  $SU(2)$ . The boundary conditions of the fermionic fields are periodic in the space directions and antiperiodic in the time direction. In the absence of a magnetic field the fermionic part of the action which we use becomes the usual staggered action,

$$S_F = a^3 \sum_{n, n'} \bar{\chi}(n) [D(n, n') + ma\delta_{n, n'}] \chi(n'), \quad (6)$$

where  $ma$  is the bare quark mass and

$$D(n, n') = \frac{1}{2} \sum_\mu \eta_\mu(n) [U_\mu(n) \delta_{n+\mu, n'} - U_\mu^\dagger(n-\mu) \delta_{n-\mu, n'}]. \quad (7)$$

The arguments  $n, n'$  are integer four-vectors denoting sites on the lattice and  $\eta_\mu(n)$  are the normal staggered sign factors,

$$\begin{aligned} \eta_1(n) &= 1, \\ \eta_\mu(n) &= (-1)^{\sum_{\nu=1}^{\mu-1} n_\nu}, \quad \mu = 2, 3, 4. \end{aligned} \quad (8)$$

We want to introduce an external constant magnetic field interacting with the fermions. We therefore introduce electromagnetic potentials in the fermion action by new, commuting group elements on the

links, namely  $V_\mu(n) = e^{i\theta_\mu(n)} \in U(1)$ . As discussed in our earlier work [17] a constant magnetic background field in the  $z \equiv 1$ -direction going through all the  $(x, y) \equiv (1, 2)$  -planes of finite size  $N_\sigma \times N_\sigma$  with a constant magnetic flux  $\phi = a^2 q B$  through each plaquette can be realized as follows:

$$\begin{aligned} V_1(n) &= e^{-i\phi n_2/2} \quad (n_1 = 1, 2, \dots, N_\sigma - 1), \\ V_2(n) &= e^{i\phi n_1/2} \quad (n_2 = 1, 2, \dots, N_\sigma - 1), \\ V_1(N_\sigma, n_2, n_3, n_4) &= e^{-i\phi(N_\sigma+1)n_2/2}, \\ V_2(n_1, N_\sigma, n_3, n_4) &= e^{i\phi(N_\sigma+1)n_1/2}, \\ V_3(n) &= V_4(n) = 1. \end{aligned} \quad (9)$$

With periodic boundary conditions the magnetic flux becomes quantized as

$$\phi = a^2 q B = \frac{2\pi N_b}{N_\sigma^2}, \quad N_b \in Z. \quad (10)$$

Thus, on the lattice there is always a minimum non-vanishing flux. Because the angle  $\phi$  is periodic, there is also a maximum flux. In fact, one has to restrict oneself to  $\phi < \pi/2$ . Inserting this in (10) one obtains the condition

$$N_b < N_\sigma^2/4. \quad (11)$$

At finite temperature thus  $\frac{\sqrt{qB}}{T}$  is restricted to the region

$$\sqrt{2\pi} \frac{N_\tau}{N_\sigma} < \frac{\sqrt{qB}}{T} < \sqrt{\frac{\pi}{2}} N_\tau. \quad (12)$$

Finally we introduce the fields  $V_\mu(\theta)$  into the fermionic action (7) by substituting

$$U_\mu(n) \rightarrow V_\mu(n) U_\mu(n), \quad (13)$$

$$U_\mu^\dagger(n) \rightarrow V_\mu^*(n) U_\mu^\dagger(n). \quad (14)$$

The partition function is given by

$$Z(\theta) = \int \prod (d\bar{\chi}(n) d\chi(n) dU_\mu(n)) e^{-S_G - S_F(\theta)}. \quad (15)$$

Note that the fields  $\theta_\mu(n)$  are not treated as dynamical variables, and that there is thus no corresponding dynamical part of the action.

To determine the lattice spacing we calculate the potential between heavy quarks on a zero temperature lattice. On the same lattice we also measure the Goldstone pion mass. Details of these calibration measurements are given in Section IV below.

To study the influence of an external magnetic field on two-color QCD at finite temperature, we first look at the anisotropy in the gluonic action by measuring the average value  $\langle P_{\mu\nu} \rangle$  of the non Abelian plaquette energies for the different combinations of directions.

We further measure the following approximate order parameters.

The chiral condensate, which is an exact order parameter in the limit of vanishing quark mass, is given by

$$\begin{aligned} a^3 \langle \bar{\chi} \chi \rangle &= -\frac{1}{V} \frac{1}{4} \frac{\partial}{\partial(ma)} \log(Z) = \\ &= \frac{1}{V} \frac{1}{4} \langle \text{Tr}(D + ma)^{-1} \rangle. \end{aligned} \quad (16)$$

The factor  $1/4$  is inserted because we define  $\langle \bar{\psi} \psi \rangle$  per flavor, and our theory has 4 flavors.

We compute also the average value of the Polyakov loop  $\langle L \rangle$ , which is the order parameter for confinement in the limit of infinite quark mass (the pure gauge theory),

$$\begin{aligned} \langle L \rangle &= \frac{1}{N_\sigma^3} \sum_{n_1, n_2, n_3} \frac{1}{2} \times \\ &\langle \text{Tr} \left( \prod_{n_4=1}^{N_\tau} U_4(n_1, n_2, n_3, n_4) \right) \rangle. \end{aligned} \quad (17)$$

It is important to notice that the mean values defined above are bare quantities which should be renormalized when comparing with continuum expectation values.

### III. SIMULATION SETUP

In the present investigation we use the fixed-scale approach, i.e. we keep  $\beta$  fixed and thereby the lattice spacing  $a$  and vary the temperature by changing  $N_\tau$ . More precisely we simulated the theory at  $\beta = 1.80$  mainly with lattice sizes  $32^3 \times N_\tau$ ,  $N_\tau = 4, 6, 8, 10$ , and with a lowest mass value  $ma = 0.0025$  taking each time at least three values of the magnetic flux,  $N_b = 0, 80, 200$ .

The simulation algorithm employed is the usual Hybrid Monte Carlo method, updated in various respects in order to increase efficiency (even-odd and mass preconditioning, multiple time scales, Omelyan integrator and written in CUDA Fortran for the use on GPU's). The number of configurations (trajectories) generated in a simulation varied between 3000 and 5000. In general, 250 configurations were discarded for initial thermalization.

We measured the chiral condensate on every third configuration, apart from  $N_\tau = 6$  and  $N_b = 80, 200$  where we used every fifth configuration only, because in these runs we are close to the transition temperature. The Polyakov loop and the plaquette variables were measured on every configuration. The chiral condensate was evaluated with the random source method. Thereby we used 100  $Z_2$  random sources per

configuration. The integrated autocorrelation times of all observables were taken into account in the error analysis. It could be estimated to be mostly well below 20 consecutive trajectories.

A zero temperature simulation with zero magnetic field was performed for the same  $\beta = 1.80$  and for the two mass values  $ma = 0.0025, 0.01$  on a lattice of size  $32^3 \times 48$  in order to estimate the lattice spacing and the pion mass. The number of trajectories in this run was about 1200 and the first 200 were discarded. Measurements were performed after every third trajectory.

#### IV. FIXING THE LATTICE SCALE

In order to determine the lattice spacing we investigate the potential between infinitely heavy quarks. We use the Sommer parameter, defined in the continuum by the equation

$$r^2 \frac{dV_S}{dr} \Big|_{r=r_0} = 1.65. \quad (18)$$

On the lattice we measure the potential using Wilson loops. In order to suppress taste symmetry breaking and to increase the signal-to-noise ratio, HYP-smearing [28] with additional APE-smearing [29] (in the version used in [30]) was applied to the gauge configurations before measurements were performed. The potential as extracted from Wilson loops is not spherically symmetric, in particular for small distances. Defining  $R$  as the distance in lattice units ( $r = Ra$ ), we introduce a more symmetric potential by

$$V(R) = V_S(R) + C\left(\frac{1}{R} - G_L(R)\right), \quad (19)$$

where  $G_L(R)$  is the free gluon propagator on the lattice. We then make the Ansatz

$$V_S(R) = A_1 - \frac{A_2}{R} + \sigma a^2 R. \quad (20)$$

The potential  $V_S(R)$  as well as the best fit are shown in Fig. 1 (left panel).

The fit parameters are given in Table I.

As the two sides in Eq. (18) are dimensionless, the same equation holds for the lattice distance  $R$ . Thus, assuming the form (20) for the potential we obtain

$$r_0/a = R_0 = \sqrt{\frac{1.65 - A_2}{\sigma a^2}}. \quad (21)$$

We are, of course, aware of the fact that we are considering a fictitious world of two-color QCD with four

flavors of quarks with equal charges  $q$ . Nevertheless, the scale determination provides a rough estimate of the magnetic field strength for the various values of the flux and the distance to the chiral limit.

Inserting the value  $r_0 = 0.468(4)$  fm [31] we obtain the lattice spacing from a fit with formula (21)

$$a = 0.168(4) \text{ fm} \quad (22)$$

for  $ma = 0.0025$  and an only slightly larger value for  $ma = 0.01$  [17] (see Table III). Through variation of the fit range we estimate the systematic error of the lattice spacing to be smaller than 10%.

To determine the Goldstone pion mass we calculate the corresponding correlator, which is given by

$$C(n_4) = \sum_{n_1, n_2, n_3} |G(n, 0)|^2, \quad (23)$$

where  $G(n, 0)$  is the quark propagator on the lattice. Though there are in principle benefits by using more complicated sources, we found that simple point sources are sufficient in our case. The effective mass

$$M_{eff}(n_4 + \frac{1}{2}) = \log \frac{C(n_4)}{C(n_4 + 1)} \quad (24)$$

was analysed to determine the range where the contribution of higher states are negligible, corresponding to a plateau in  $M_{eff}(n_4)$ . See middle and right panels of Fig. 2.

In the plateau range we measure the Goldstone pion mass from a fit to the correlator (23) of the form

$$C_\pi(t) = C(e^{-Et} + e^{E(t-N_\tau)}), \quad (25)$$

where  $t \equiv n_4$  and  $E = m_\pi a$ . We obtain a clear plateau in the effective mass and a very good fit for  $t_{min} = 7$ , as can be seen in Table II.

Inserting the value of  $a$  from (22) in the result for  $E$  leads to

$$m_\pi = 175(4) \text{ MeV}, \quad (26)$$

for  $ma = 0.0025$  which is, as expected from the phenomenological rule  $m_\pi^2 \propto m_q$ , about half the value obtained for  $ma = 0.01$  [17] (cf. Table III). As we will see below, we now have  $m_\pi \approx T_c(B = 0)$ . Therefore, we expect that our results will be relevant to the physical case of QCD.

#### V. RESULTS

We start by discussing the influence of the temperature and magnetic field on the different parts  $P_{\mu\nu}$  of the gluonic action. For convenience we introduce similar variables as in [24]:

$$\mathcal{E}_i^2 = P_{4i}, \quad (27)$$

$$\mathcal{B}_i^2 = |\epsilon_{ijk}| P_{jk}, \quad j < k. \quad (28)$$

At  $B = T = 0$  they are all equal by symmetry. At  $B = 0, T \neq 0$  they fall into two groups, because the fourth direction is not equivalent to the other ones:

$$\mathcal{E}_1^2 = \mathcal{E}_2^2 = \mathcal{E}_3^2, \quad (29)$$

$$\mathcal{B}_1^2 = \mathcal{B}_2^2 = \mathcal{B}_3^2. \quad (30)$$

Introducing a magnetic field in the third direction, for  $T \neq 0$  the only symmetries left are rotations in the  $(1, 2)$ -plane. We therefore may define

$$\mathcal{E}_\parallel^2 \equiv \mathcal{E}_3^2, \quad (31)$$

$$\mathcal{E}_\perp^2 \equiv \mathcal{E}_1^2 = \mathcal{E}_2^2, \quad (32)$$

$$\mathcal{B}_\parallel^2 \equiv \mathcal{B}_3^2, \quad (33)$$

$$\mathcal{B}_\perp^2 \equiv \mathcal{B}_1^2 = \mathcal{B}_2^2. \quad (34)$$

In Fig. 2 we show the results for the four values of the temperature, and each of them for the three values of the magnetic field. We give them in physical units by using Eq. (22).

We can see the following features from this figure. The pattern of the splitting is the same as in our earlier article [17] and more recently found in full QCD [24],

$$\langle \mathcal{B}_\parallel^2 \rangle \geq \langle \mathcal{B}_\perp^2 \rangle \geq \langle \mathcal{E}_\perp^2 \rangle \geq \langle \mathcal{E}_\parallel^2 \rangle. \quad (35)$$

Furthermore, when the values of  $\langle \mathcal{B}_\perp^2 \rangle$  and  $\langle \mathcal{E}_\perp^2 \rangle$  become different from each other, the system can be expected to be at the onset of the deconfinement transition or even inside the deconfined phase. If we compare the middle panel ( $qB = 0.67 \text{ GeV}^2$ ) of Fig. 2 with the left one ( $qB = 0$ ) then at  $T = 195 \text{ MeV}$  ( $N_\tau = 6$ ) we find this difference to be slightly larger than for the left panel. This might be an indication that the transition temperature as a function of the temperature went down a bit with increasing magnetic field strength (*inverse magnetic catalysis*). However, comparing the right-most panel ( $qB = 1.69 \text{ GeV}^2$ ) with the left one, then the corresponding difference is definitely smaller than for zero magnetic field. This indicates that the transition might be shifted to a higher temperature value (*magnetic catalysis*).

In Fig. 3 (left) the expectation value of the unrenormalized Polyakov loop  $\langle L \rangle$  is shown as a function of the temperature. Our values  $N_\tau = 10, 8, 6, 4$  correspond to temperature values  $T$ , which are quite widely spaced. Therefore, we cannot localize the transition e.g. for  $B = 0$  very well. It happens around  $T = T_c \simeq 160 - 200 \text{ MeV}$ . This means that  $T_c \simeq m_\pi$ , like in QCD. We also observe a curious pattern at  $T = 195 \text{ MeV}$  ( $N_\tau = 6$ ), namely that the Polyakov loop does not behave monotonously with the magnetic field. We will come back to that behavior later. We are aware of the fact, that a proper renormalization of the Polyakov loop with respect to the  $N_\tau$ -dependence will weaken the steep rise with  $T$ . However, our main

conclusions concerning the  $qB$ -dependence at fixed  $T$ -values will remain unchanged.

In Fig. 3 (right) the unrenormalized chiral order parameter  $a^3 \langle \bar{\psi} \psi \rangle$  is shown versus  $T$ . We observe that for a fixed non-vanishing quark mass it grows monotonously with the magnetic field at least for all the four temperature values we have investigated. This might mean that  $T_c$  always increases with a rising magnetic field strength as required for the *magnetic catalysis*. In particular at  $T = 195 \text{ MeV}$  we observe a strong increase of the condensate in between  $qB = 0.67 \text{ GeV}^2$  and our largest value  $1.69 \text{ GeV}^2$  showing that the system ‘jumps’ from chiral symmetry restoration to the chirally broken phase. This indicates that at this temperature value and within the given range of magnetic field strength values the critical  $T_c(B)$  is rising.

Indeed, we find this confirmed in Fig. 4, where  $a^3 \langle \bar{\psi} \psi \rangle$  is shown as a function of the bare quark mass  $ma$  at two temperatures,  $T = 147$  and  $195 \text{ MeV}$ , respectively. One may use these data to extrapolate  $a^3 \langle \bar{\psi} \psi \rangle$  down to the chiral limit. For  $T = 147 \text{ MeV}$  we are clearly in the chirally broken phase for all values of  $B$  including  $B = 0$ . However, at the higher temperature  $T = 195 \text{ MeV}$  the condensate  $a^3 \langle \bar{\psi} \psi \rangle$  extrapolates to zero for  $qB = 0$  and  $0.67 \text{ GeV}^2$  corresponding to the chirally restored phase, while for the stronger magnetic field strength  $1.69 \text{ GeV}^2$  the data suggest a non-vanishing chiral condensate in the chiral limit. Thus, we may conclude that at very strong magnetic field values the transition temperature grows with  $B$ . This means *magnetic catalysis* in agreement with various models [10].

In order to study the situation in more detail, we have made simulations at fixed  $N_\tau = 6$  ( $T = 195 \text{ MeV}$ ) and seven values of  $N_b$ . The latter correspond to a range of  $qB$  between 0 and  $1.69 \text{ GeV}^2$ . We measure the expectation values of the Polyakov loop and the chiral condensate. The results are shown in Fig. 5. There is a sharp change, which might be related to a phase transition in the range  $0.7 \text{ GeV}^2 < qB < 1.0 \text{ GeV}^2$  corresponding to  $\sqrt{qB}/T \approx 4.5$ . This observation is supporting a *magnetic catalysis* phenomenon. But for lower magnetic fields we observe a **rise of the Polyakov loop** with  $qB$  towards the transition and only then a drop off followed by a monotonous decrease at larger field values (compare with our previous comment to Fig. 3 (left)). The rise at low magnetic field values might mean that we are going deeper into the deconfinement region, after which the transition brings us back into the confinement or chirally broken phase. The reader should keep in mind that these data are all obtained at fixed quark mass  $am = 0.0025$ . There the chiral condensate (see the right panel of Fig. 5) rises also at a weak field  $qB$ . However, in this deconfinement range the chiral condensate is anyway expected to vanish in the chiral limit. The observation of the rise of the Polyakov

loop at low magnetic field values resembles the pattern discussed in Ref. [25]. It leaves some space for a decrease of  $T_c$ , i.e. for an *inverse magnetic catalysis* also in two-color QCD considered throughout this work. In Fig. 6 we conjecture a  $B - T$  phase diagram, which might clarify the situation. In order to prove it, further simulations at somewhat smaller temperatures and/or smaller quark mass would be helpful.

## VI. CONCLUSIONS

In this article we have described an investigation of two-color QCD at finite temperature in a constant external magnetic field. We specialized to the case of four flavors of equal charge  $q$  implementing staggered fermions on the lattice without employing the fourth root trick, the latter being still under debate. We have performed lattice simulations using a fixed-scale approach so that we do not need to know the beta-function and the dependence of the renormalization constants on the bare coupling constant. The simulations were performed at a lattice spacing  $a \approx 1/(6 T_c(0))$ , where  $T_c(0)$  is the critical temperature of the finite temperature transition at vanishing magnetic field. Furthermore, we used a fixed bare quark mass which is four times smaller than in our previous work [17]. This means that now the Goldstone meson mass is  $m_\pi \approx T_c(0)$  similar to the physical case of QCD. We have also taken some data at larger quark masses to be able to extrapolate to the chiral limit.

We find that at sufficiently large magnetic fields there is *magnetic catalysis*, i.e. the chiral order parameter and the critical temperature are increasing with increasing magnetic field strength. This is in agreement with predictions by many models. The result is, however, apparently different from that of Ref. [21] close to the physical point of QCD, where one finds *inverse magnetic catalysis*, i.e. in the transition region the chiral order parameter is not increasing monotonically with the magnetic field strength, and as a consequence the transition temperature decreases. Since our theory is different there is no discrepancy in principle but the response of the system to a strong magnetic field should be to some extent model independent for models with similar chiral properties.

We note, however, that the magnetic field strength at which we see a clear signal of magnetic catalysis is (to the extent one can compare scales in different theories) larger than those investigated in [21]. At a magnetic field strength similar to those used in [21] our data are at least consistent with an inverse magnetic catalysis scenario. Thus, e.g. in [25] it is claimed that the inverse magnetic catalysis is due to the coupling of the magnetic field to the sea quarks. This also gives rise to an increase in the Polyakov loop with the magnetic field strength, which is an effect that we see in our calculations up to a critical magnetic field, where the Polyakov loop suddenly drops to a value near zero, and the system enters the confined phase. This critical magnetic field is stronger than those used in [21, 25].

As always in lattice calculations it is possible that, although at present the bare parameters are similar in the two investigations, the results may change when the calculations approach the chiral and continuum limit. In our calculations we use four flavors and an unimproved fermionic action. In [21] a stout fermion action and the fourth root trick is used. Thus, on the lattice the sea quark content is different. This is true also in the continuum limit.

It would be very interesting to have results from QCD calculations at stronger magnetic fields to see if the phase diagram of [21] extends to the one we propose in Fig. 6, or if the inverse magnetic catalysis persists for all values of the magnetic field strength.

A further simulation of our model at a somewhat lower temperature would be important to pinpoint the critical line in the phase diagram. Investigations at different quark masses  $ma$  would be important, because the phase transition line is expected to depend on the quark mass. Finally, an extension of our calculations to smaller scales  $a$  would, of course, also be important in order to take the continuum limit.

## Acknowledgments

Useful discussions with F. Bruckmann, M. D'Elia, T. Kovacs, E. Laermann and a correspondence with L. McLerran are gratefully acknowledged. We thank F. Burger for continuous technical help and advice, in particular for running our CUDA codes on a PC cluster with GPU's.

- 
- [1] D. Kharzeev, L. McLerran, and H. Warringa, Nucl.Phys. **A803**, 227 (2008), 0711.0950.
  - [2] V. Skokov, A. Illarionov, and V. Toneev, Int.J.Mod.Phys. **A24**, 5925 (2009), 0907.1396.
  - [3] L. McLerran and V. Skokov (2013), 1305.0774.
  - [4] J. Geheniau, Physica **Haag** **16**, 822 (1950).
  - [5] Y. Katayama, Prog. Theor. Phys. **6**, 309 (1951).
  - [6] J. Schwinger, Phys.Rev. **82**, 664 (1951).
  - [7] S. Klevansky and R. Lemmer, Phys.Rev. **D39**, 3478 (1989).
  - [8] I. Shushpanov and A. Smilga, Phys.Lett. **B402**, 351 (1997), hep-ph/9703201.

- [9] V. Gusynin, V. Miransky, and I. Shovkovy, *Phys.Rev.Lett.* **73**, 3499 (1994), hep-ph/9405262.
- [10] I. A. Shovkovy, *Lect.Notes Phys.* **871**, 13 (2013), 1207.5081.
- [11] N. Agasian, *Phys.Atom.Nucl.* **64**, 554 (2001), hep-ph/0112341.
- [12] N. Agasian and S. Fedorov, *Phys.Lett.* **B663**, 445 (2008), 0803.3156.
- [13] P. Buividovich, M. Chernodub, E. Luschevskaya, and M. Polikarpov, *Phys.Lett.* **B682**, 484 (2010), 0812.1740.
- [14] P. Buividovich, M. Chernodub, E. Luschevskaya, and M. Polikarpov, *Nucl.Phys.* **B826**, 313 (2010), 0906.0488.
- [15] P. Buividovich, M. Chernodub, E. Luschevskaya, and M. Polikarpov, *Phys.Rev.* **D80**, 054503 (2009), 0907.0494.
- [16] P. Buividovich, M. Chernodub, E. Luschevskaya, and M. Polikarpov, *Phys.Rev.* **D81**, 036007 (2010), 0909.2350.
- [17] E.-M. Ilgenfritz, M. Kalinowski, M. Müller-Preussker, B. Petersson, and A. Schreiber, *Phys.Rev.* **D85**, 114504 (2012), 1203.3360.
- [18] M. D’Elia, S. Mukherjee, and F. Sanfilippo, *Phys.Rev.* **D82**, 051501 (2010), 1005.5365.
- [19] M. D’Elia and F. Negro, *Phys.Rev.* **D83**, 114028 (2011), 1103.2080.
- [20] C. Bonati, M. D’Elia, M. Mariti, F. Negro, and F. Sanfilippo (2013), 1307.8063.
- [21] G. Bali, F. Bruckmann, G. Endrodi, Z. Fodor, S. Katz, et al., *JHEP* **1202**, 044 (2012), 1111.4956.
- [22] G. Bali, F. Bruckmann, G. Endrodi, Z. Fodor, S. Katz, and A. Schäfer, *Phys.Rev.* **D86**, 071502 (2012), 1206.4205.
- [23] G. Bali, F. Bruckmann, M. Constantinou, M. Costa, G. Endrodi, et al., *Phys.Rev.* **D86**, 094512 (2012), 1209.6015.
- [24] G. Bali, F. Bruckmann, G. Endrodi, F. Gruber, and A. Schäfer, *JHEP* **1304**, 130 (2013), 1303.1328.
- [25] F. Bruckmann, G. Endrodi, and T. Kovacs, *JHEP* **1304**, 112 (2013), 1303.3972.
- [26] S. Borsanyi et al., *JHEP* **11**, 077 (2010), 1007.2580.
- [27] M. D’Elia, *Lect.Notes Phys.* **871**, 181 (2013), 1209.0374.
- [28] A. Hasenfratz and F. Knechtli, *Phys. Rev.* **D64**, 034504 (2001), hep-lat/0103029.
- [29] M. Albanese et al. (APE), *Phys. Lett.* **B192**, 163 (1987).
- [30] V. Bornyakov, E. M. Ilgenfritz, and M. Müller-Preussker, *Phys. Rev.* **D72**, 054511 (2005), hep-lat/0507021.
- [31] A. Bazavov, T. Bhattacharya, M. Cheng, C. Detar, H. Ding, et al., *Phys.Rev.* **D85**, 054503 (2012), 1111.1710.

$\beta$	$am$	$N_\sigma$	$N_\tau$	$R_{min}$	$R_{max}$	$A_1$	$A_2$	$\sigma$	$\chi^2_{dof}$
1.8	0.01	16	32	1.2	3.2	0.265(38)	0.370(42)	0.169(8)	0.87
1.8	0.0025	32	48	1.2	3.0	0.078(24)	0.152(21)	0.192(7)	1.16

TABLE I: Fit parameters in lattice units for the static potential  $V_S(R)$  acc. to Eq. (20) for two sets of parameters considered in [17] and in this work.  $R_{min}$  and  $R_{max}$  define the fitrange for the static potential in lattice units.

$\beta$	$am$	$N_\sigma$	$N_\tau$	$t_{min}$	$C_0$	$E = am_\pi$	$\chi^2_{dof}$
1.8	0.01	16	32	6	1.01(3)	0.285(1)	0.023
1.8	0.0025	32	48	7	1.58(8)	0.149(3)	0.010

TABLE II: Fit parameters in lattice units for the pion correlator  $C_\pi(t)$  according to Eq. (25) for the two sets of simulation parameters considered in [17] and in this work. The fit range for the pion correlator starts at lattice distance  $t_{min}$ .

$\beta$	$am$	$N_\sigma$	$N_\tau$	$N_{b,max}$	$R_0$	$a[\text{fm}]$	$m_\pi[\text{MeV}]$	$\sqrt{qB_{max}}[\text{GeV}]$
1.8	0.01	16	32	50	2.75(8)	0.170(5)	330(10)	1.29(4)
1.8	0.0025	32	48	200	2.78(6)	0.168(4)	175(4)	1.30(3)

TABLE III: Results for the Sommer scale  $R_0$  (in lattice units), the lattice spacing  $a$ , the pion mass  $m_\pi$ , and the quantity  $\sqrt{qB_{max}}$  characterizing the magnetic field strength for the largest number of flux units  $N_{b,max}$  used for various setups of simulation parameters considered in [17] and this work.

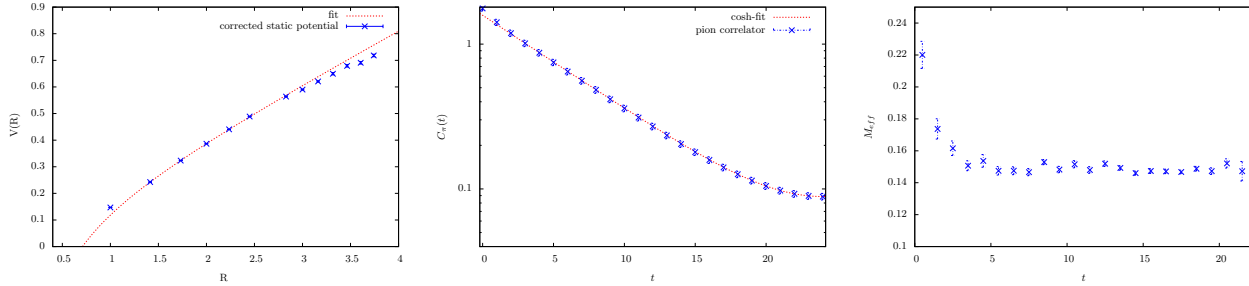


FIG. 1: Potential of a static quark-antiquark pair (left), pion correlator (middle) and effective mass  $M_{eff}(t)$  (right) all measured at  $\beta = 1.80$  and bare quark mass  $am = 0.0025$ . The lattice size is  $32^3 \times 48$ . The dotted line in the left panel corresponds to a fit the parameters of which are given in Table I.

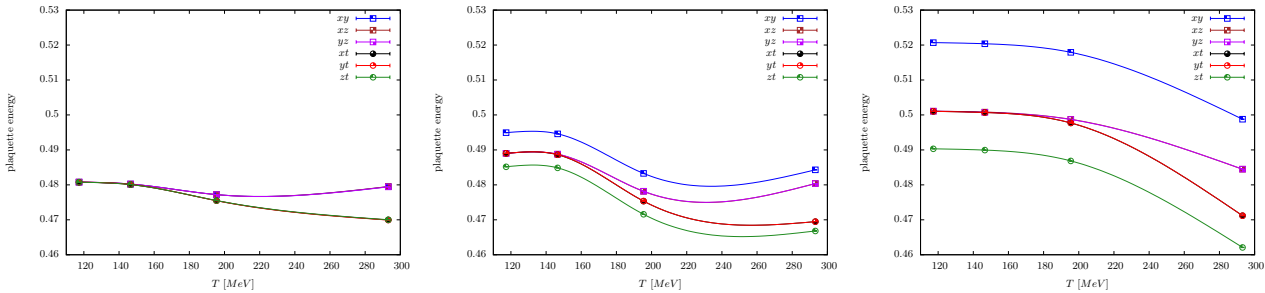


FIG. 2: Plaquette energies  $\langle P_{\mu\nu} \rangle$  vs. temperature  $T = (a(\beta)N_\tau)^{-1}$  without magnetic field (left panel), with  $qB = 0.67 \text{ GeV}^2$  (middle) and  $qB = 1.69 \text{ GeV}^2$  (right panel) for the different plaquette orientations. The lines are only to guide the eye. Computations were done for  $\beta = 1.80$ ,  $am = 0.0025$ ,  $N_\sigma = 32$ .



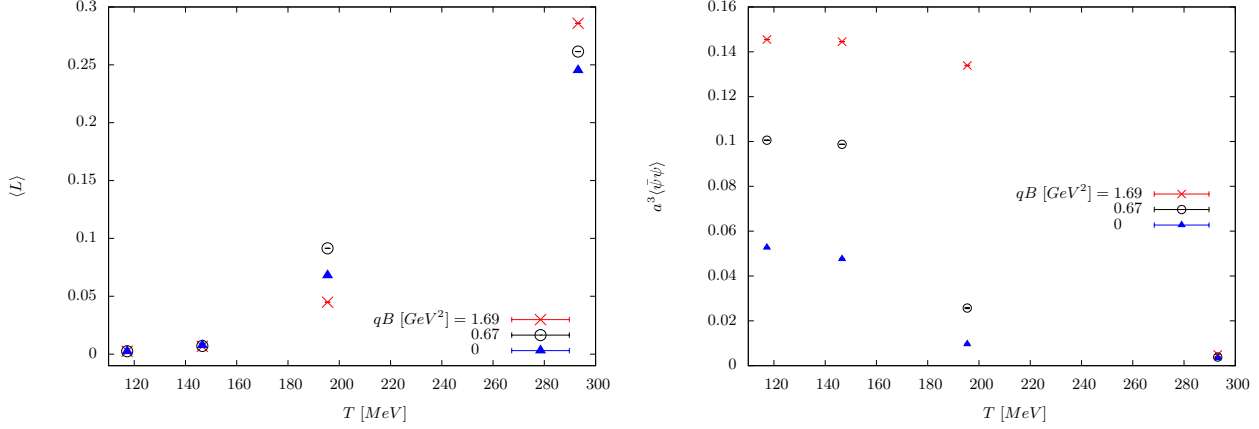


FIG. 3: Bare Polyakov loop  $\langle L \rangle$  (left) and bare chiral condensate  $\langle \bar{\psi}\psi \rangle$  (right) vs. temperature  $T = (a(\beta)N_\tau)^{-1}$  shown for three values of the magnetic field strength at  $\beta = 1.80$ ,  $am = 0.0025$  and lattice sizes  $32^3 \times N_\tau$ ,  $N_\tau = 4, 6, 8, 10$ .

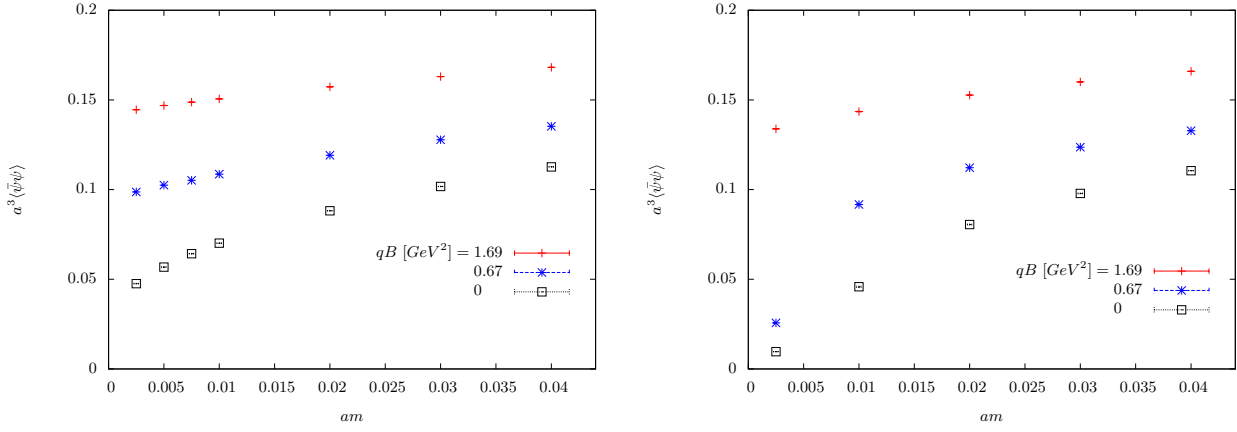


FIG. 4: Mass dependence of the bare chiral condensate  $\langle \bar{\psi}\psi \rangle$ . Data points are shown for  $N_\tau = 8$ , i.e.  $T = 147$  MeV (left panel) and for  $N_\tau = 6$ , i.e.  $T = 195$  MeV (right panel), in each case for three values of the magnetic field. The simulations were done with  $\beta = 1.80$  and spatial linear lattice extent  $N_\sigma = 16$ , except for the three smallest mass values  $am = 0.0025, 0.0050, 0.0075$ , where  $N_\sigma = 32, 24, 20$ , respectively, was chosen.

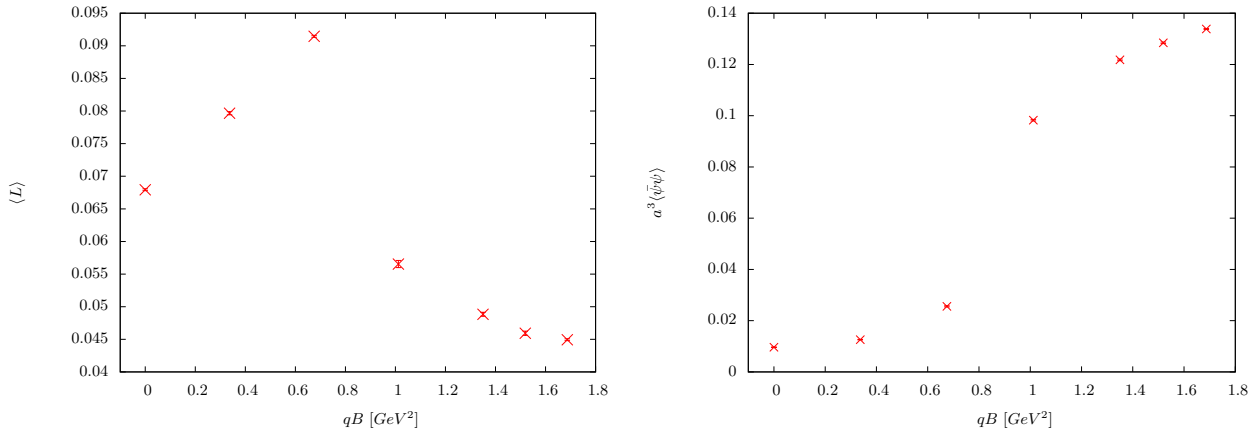


FIG. 5: Polyakov loop (left panel) and chiral condensate (right panel) vs. field strength  $qB$  at  $T = 195$  MeV obtained with  $\beta = 1.80$ ,  $am = 0.0025$  and lattice size  $32^3 \times 6$ .

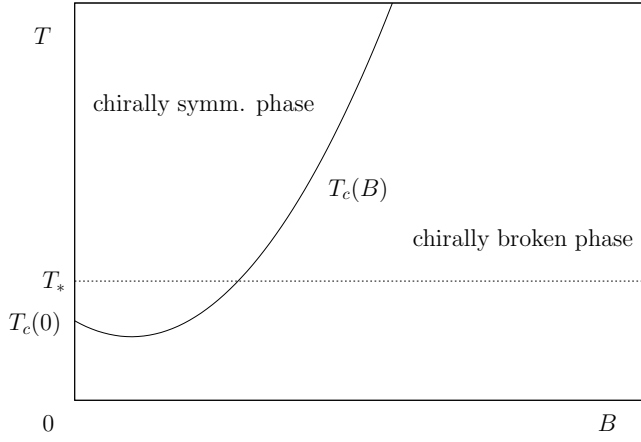


FIG. 6: Conjectured B-T phase diagram at fixed mass  $am = 0.0025$ . The horizontal line  $T = T_* = \text{const.}$  indicates the path of simulations at  $T = 195$  MeV as in Fig. 5.